



Crack paths in smooth and precracked specimens subjected to multiaxial cyclic stressing

Nicholas R. Gates

Mechanical, Industrial and Manufacturing Engineering Department, The University of Toledo, 2801 W. Bancroft Street, Toledo, OH 43606, USA
ngates@eng.utoledo.edu

Ali Fatemi

Mechanical, Industrial and Manufacturing Engineering Department, The University of Toledo, 2801 W. Bancroft Street, Toledo, OH 43606, USA
afatemi@eng.utoledo.edu

ABSTRACT. The understanding of shear-mode crack growth mechanisms and crack branching phenomena is of great interest for a variety of practical engineering situations. Despite this fact, relatively little research is available regarding these topics. Of the studies that have been performed, few provide a means of quantifying such effects and most consider crack growth starting from a precrack. The current study is aimed at trying to fill some of the research voids in these areas by investigating the effects of microcrack coalescence, loading level, and superimposed normal stresses on the mode II crack behavior of naturally initiated fatigue cracks. Based on the experimental results and subsequent analyses, it was determined that microcrack networks and coalescence have little to no effect on the experimentally observed crack paths regardless of the applied loading level. Instead, the preferred crack growth mode is shown to have a dependence on the applied shear stress magnitude and stress normal to the crack plane, indicating a significant role of friction and roughness induced crack closure effects in the crack growth process. A simple model is then proposed to quantify these effects based on the idea that crack face interaction reduces the effective mode II SIF by allowing a portion of the nominally applied loading to be transferred through a crack. The model agrees qualitatively with the experimentally observed trends for pure torsion loading and predicts crack branching lengths within a factor of 2 for all loadings considered.

KEYWORDS. Fatigue; Crack Growth; Mode II; Friction; Branching; Closure.

INTRODUCTION

Fatigue crack growth often represents a significant portion of a component's total fatigue life. Therefore, a fundamental understanding of the mechanisms that govern crack propagation and the development of accurate crack growth modeling techniques are essential to a complete fatigue life analysis. This is especially true in



situations where a damage tolerant design philosophy has been employed. Crack growth mechanisms and their influence on crack growth rate have been researched extensively over the years for uniaxial loadings and mode I crack extension. Most of these studies, however, utilize specimens which promote ideal crack growth conditions. In practical applications, where components are often subjected to complex multiaxial loading histories, these ideal conditions usually don't exist. Instead, naturally initiated fatigue cracks can grow in a complex and mixed-mode manner which is not easy to predict or quantify.

One of the complexities involved in mixed-mode crack growth is predicting crack path by determining in what direction a crack will grow throughout different stages of its development [1]. For example, cracks initiated naturally at a mechanical notch tend to nucleate and grow a short distance, usually comparable to the length of a few grains, on planes of maximum shear, but almost always turn so that long crack growth occurs on planes of maximum tensile stress [2–5]. In this case, well established mode I crack extension models can be employed to predict growth rates for a given loading history. On the other hand, long cracks in un-notched (smooth) specimens have been shown to propagate on maximum shear planes, maximum tensile planes, or a combination of both. The preferred growth plane has been shown to depend on material, nominally applied loading, and/or loading magnitude [6]. In general, cracks in the low cycle fatigue regime tend to grow on maximum shear planes while cracks at longer lives tend to transition into mode I growth [7–11].

One explanation offered for the discrepancy between crack growth in smooth and notched specimens is that a fundamental difference in crack growth mechanism exists. In the smooth specimens, the uniformly stressed gage section allows for a large number of microcracks to develop and form “crack networks” across the specimen surface. The growth of these cracks is driven primarily by far field stresses and plasticity of the gage section. Each small crack can grow to a different length and at a different rate due to microstructural variations, shielding, and other interaction with adjacent cracks in the network. These cracks grow individually and remain relatively small until near fracture where they coalesce to form a failure crack which retains the same orientation of the individual cracks. Shamsaei and Fatemi [12] observed that the development of microcrack networks in smooth specimens is more prominent in the low cycle fatigue regime due to increased plasticity in the gage section activating more slip systems. This observation agrees with the higher tendency for macroscopic shear-mode crack growth in this regime. They also observed a larger number of microcracks initiating in more ductile behaving materials, as opposed to higher strength materials, for solid cylindrical specimens, as opposed to tubular specimens, and for in-phase axial-torsion loadings, as opposed to 90° out-of-phase loadings.

For the notched specimens, in contrast to the smooth, only a small number of dominant cracks nucleate at the location(s) of maximum stress around the notch, typically on the maximum shear plane. With the absence of microcrack networks, unable to develop in the lower stressed material surrounding the notch, the cracks quickly turn into the mode I direction and grow independently, driven by the stress and plasticity fields at the crack tip. Therefore, cracks initiated from notches generally grow in a continuous manner and lack the retardation or acceleration effects observed for the smooth specimens due to crack interaction. This is also the case for cracks growing in smooth specimens tested at lower stress amplitudes. As early as the 1950s, Marco and Starkey [13] noted a difference between these two types of crack growth mechanisms and termed the growth of long cracks through microcrack coalescence a type R crack system, whereas crack growth dominated by the propagation of a single crack was termed a type S crack system.

Knowing by which mechanisms and on which planes a crack will grow is essential to performing accurate crack growth analysis. There are many parameters that can influence mixed-mode crack growth behavior, some of which include loading magnitude and R ratio, loading sequence, material strength, and crack closure [14]. To account for these effects, several prediction models or correlation parameters for both mixed-mode growth direction and growth rate have been proposed. For example, the maximum tangential stress criterion [15] has been found to give close predictions of the experimentally observed crack growth path [3], and equivalent stress intensity factor parameters, such as that proposed by Tanaka [16] can satisfactorily correlate the experimental growth rate data [4]. However, these models are most effective in the absence of crack coalescence and cannot account for differences in crack path for such cases. For example, the maximum tangential stress criterion would predict a mode II crack initiated under pure torsion loading to immediately branch at an angle of 70.5° to the crack growth direction and grow in mode I regardless of the applied loading magnitude [8, 17]. This prediction is not in agreement with the shear-mode crack growth observed in many smooth specimens from initiation up until fracture.

Owing to the complexity of the task, little research is available on models which attempt to quantify when or if cracks will grow by type R mechanisms, type S mechanisms, or whether or not these two mechanisms are even responsible for the differences in smooth and notched specimen crack paths. To simplify this problem for the following discussion, it will be assumed that naturally occurring fatigue cracks always tend to initiate on planes of maximum shear stress. This is an assumption backed by both the physics of fatigue crack initiation and by large amounts of experimental evidence [12].



This then leaves two possibilities for subsequent crack growth; the crack can either branch and grow in mode I on maximum tensile planes, or the crack can remain coplanar and grow in mode II or mixed-mode conditions until failure.

Concerning the first possibility, there is a reasonable amount of literature available describing the processes governing the transition from stage I to stage II crack growth. Murakami and Takahashi [17] studied the behavior of small mode II cracks growing under near threshold conditions for pure torsion loading of medium carbon steel solid cylindrical specimens. They observed three different conditions for crack growth from a precrack. Cracks either started to grow in both modes I and II from the precrack tip, with the mode II cracks stopping after a short distance to give way to the more dominant mode I cracks, or only mode I cracks were observed to grow from the precrack tip, or the crack propagated in mode II for a short distance before eventually branching to grow in mode I. Crack branching was attributed to a higher threshold stress intensity factor (SIF) value for modes II and III as compared to mode I. They argued that this led to an arrest of shear-mode cracks as they dropped below their threshold value which gave way to mode I growth as cracks were still above the mode I threshold SIF value [7]. They concluded that the mode I SIF of the branched cracks governed the fatigue limit for small cracks in torsion and were able to predict the fatigue limit using an extension of the square root of area parameter [17].

Makabe and Socie [18] studied crack growth in precracked specimens of 4340 steel under torsion loading with and without the influence of static axial stresses. They observed that cracks grew longer in mode II before branching as the applied shear strain and/or static axial stress increased. This was attributed to decreased contact and friction between opposing crack faces and the resulting change in slip band density surrounding the crack tip. The eventual branching mechanism was described as a zig-zagging between perpendicular slip bands generated in the vicinity of the crack tip. It was concluded that in order for a crack to continue to grow in shear-mode, the driving force for shear deformation at the crack tip must be large enough to overcome the friction between crack faces.

Considering the effects of crack face friction, Tong *et al.* [19] proposed a model to describe changes in local stress intensity factors during shear-mode crack growth based on an idealized crack face asperity angle and coefficient of friction. The model was developed for a two-dimensional edge crack growing nominally in pure mode II and relates theoretical crack sliding displacements computed using finite element analysis (FEA) to local displacement components due to wedging of crack face asperities. The local displacements are then used to compute a local reduction in mode II SIF due to friction and a local increase in mode I SIF due to wedging. Comparing the effective mode II SIF to the local mode I SIF provides a means of predicting crack branching. The model predictions were not compared directly to experimental results, but the predicted trends agreed with experimental observations. In an extension of the same work [20], the model was applied to mixed-mode I and II loadings and could be extended to other crack geometries as well, provided the appropriate weight functions and crack face loading distributions are known.

More recently, Künkler *et al.* [21] predicted the two-dimensional crack propagation behavior of short cracks under uniaxial loading in the region of stage I to stage II transition using a microstructure sensitive modeling technique. They found that mode II growth occurs primarily on single slip systems within individual grains. Once the crack reaches a length where its plastic zone is large enough to activate additional slip systems in neighboring grains, the crack begins to transition to mode I growth by switching from a single slip mechanism to a double slip propagation mechanism. In double slip crack growth, shear displacements on the two different slip systems cause a crack tip opening which promotes mode I crack extension. The crack length at this transition was considered dependent upon crack geometry, grain size, and the orientation of slip systems in neighboring grains.

In 2014, Pokluda *et al.* [10] reviewed research on shear-mode crack behavior in metallic materials. It was concluded that the main factor driving the branching of mode II cracks is crack face friction and wedging caused by surface asperities. These asperities result from microstructural level crack meandering due to differing orientations of slip systems, and their average inclination angle was shown to vary based on the crystallographic structure of the material. When mode II sliding displacements occur between opposing crack faces, the wedging effect of these asperities acts to simultaneously reduce the effective value of the mode II SIF and introduce a local mode I SIF component. When the conditions are such that the local mode I SIF value exceeds the mode I threshold, crack branching is considered to occur. The authors applied a simple crack branching criterion to predict whether or not crack branching would occur in the threshold region before a crack became non-propagating. They compared the predictions to experimental data of four different metals and reported good agreement.

While the aforementioned studies deal with describing or predicting the development of a mode I branch from a mode II crack in the near threshold regime, far less literature is available concerning the conditions for continuous coplanar shear-mode propagation of a crack. Tschegg [11] discussed this issue in a study of mode III crack growth behavior in circumferentially grooved cylindrical specimens of 4340 steel. The change in fracture mode was found to coincide with the intersection of the mode I and mode III crack growth curves. At lower stress intensity values, where crack branching and



factory roof fracture surfaces were observed, it was speculated that the mode I loading of favorably oriented microcracks in the crack tip plastic zone would produce higher crack growth rates than the effective mode III loading of the main crack. Therefore, whichever loading mode produced the highest crack growth rate values for a given combination of loading conditions and crack length was considered to control the crack growth process.

Using a similar “maximum growth rate” approach, Doquet and Bertolino [8] addressed the fracture mode issue by considering a local approach based on elastic-plastic crack tip stresses and strains derived via non-linear incremental FEA. Two multiaxial fatigue damage parameters, one predicting tensile dominated failure (Smith-Watson-Topper) and one predicting shear dominated failure (Fatemi-Socie) were then applied to predict crack path based on which mode would produce the most damage (based on the shortest predicted life and highest growth rate). The damage parameter values were averaged over an arbitrary length (between 0.020 – 0.100 mm) along a radial line emanating from the crack tip along either plane experiencing the maximum normal strain or maximum shear strain range. A transition in growth mode from tensile dominated to shear dominated was successfully predicted at higher applied loading, but no quantitative comparison was made to experimental results. A major drawback of this approach, however, is the need to perform non-linear FEA over an entire cycle for each crack length and loading level being considered.

Tanaka [9], in an investigation on shear crack growth in circumferentially grooved specimens of a stainless and carbon steel, speculated that a criterion for coplanar versus branched crack growth could be related to the shear strain range ahead of the crack tip. For higher loading levels, it was suggested that increased plasticity at the crack tip could lead to the initiation of local shear oriented microcracks ahead of the crack tip which would encourage coplanar crack growth through local coalescence. However, no quantitative analysis was provided.

This study is similar in some regards to those mentioned previously, but presents some aspects typically not considered in shear-mode crack growth studies. For example, nearly all of the aforementioned studies deal exclusively with mode II cracks growing from precracks or circumferential notches. This study, on the other hand, places a strong emphasis on the behavior of naturally initiated fatigue cracks in smooth specimens. One problem with studying growth from precracks is that residual stresses in the crack tip region, resulting from the precracking procedure, have the potential to influence the subsequent mode II crack growth. Even if specimens are annealed following precracking to eliminate these effects, the crack face topography still varies from that of a naturally occurring crack. In addition, growing a mode II crack from a precrack can significantly alter the length scale required for branching mechanisms to occur and eliminates any influence on crack path from microcrack coalescence. The present study compares crack path evolution between both natural cracks and cracks growing from artificial precracks in order to evaluate the effect of microcrack coalescence on overall crack path. The role of crack face friction and roughness induced crack closure on shear-mode crack growth is evaluated as well. An emphasis is placed on crack paths in the low to intermediate fatigue life regime where mode II cracks may or may not branch to grow in mode I. In an attempt to quantify the experimental observations, a model is proposed to account for reductions in effective mode II SIF due to crack face interaction effects.

MATERIAL AND TESTING PROCEDURES

All tests performed for this study utilized thin-walled tubular specimens of 2024-T3 aluminum alloy, a common aerospace alloy since the 1930s. Mechanical properties for the material were generated experimentally and include a yield strength (0.2% offset) of 330 MPa, ultimate tensile strength of 495 MPa, and modulus of elasticity of 73.7 GPa. The specimens, machined from drawn tubing with nominal dimensions of 34.9 mm outside diameter and 4.75 mm wall thickness, were designed in accordance with ASTM Standard E2207 [22] and feature a 30 mm long gage section with an outside diameter of 29 mm and an inside diameter of 26 mm, resulting in a wall thickness of 1.5 mm. The specimen geometry and dimensions are shown in Fig. 1(a). For precracked specimens, the term precrack is used to refer to a small notch machined in the specimen meant to resemble, as closely as possible, the profile of a naturally occurring fatigue crack. No actual precracking procedure was performed on this notch prior to applying the testing loads. It is referred to as a precrack simply as a means of differentiating it from other notched specimens, containing non crack-like notches, which are referred to in the introduction. All precrack notches were machined by means of a 0.127 mm diameter ball mill and were semi-elliptic in shape. The precracks were of a length and depth equal to approximately 1 mm and 0.2 mm, respectively, and were aligned with a plane of maximum shear stress for each applied loading condition. A sectioned view of a precrack notch is shown in Fig. 1(b). All smooth specimens were fully polished, inside and out, to eliminate any adverse effects from machining marks. Final polishing was performed with a 3 micron lapping film. Precracked specimens were polished similarly, but external polishing was only performed in the crack growth region surrounding the precrack.

All fatigue tests were carried out in a closed loop servo-hydraulic axial–torsion load frame with a dynamic rating of 100 kN axial load and 1 kN·m torsional load. Load train alignment was verified in accordance with ASTM Standard E1012 [23] prior to the beginning of, and periodically throughout, testing. Crack initiation and growth were monitored via cellulose acetate replication for smooth specimen tests, and by using a 2.0 megapixel digital microscope camera, capable of 10–230x optical zoom levels, for precracked specimens. Crack lengths were measured using an eyepiece scale affixed to an optical microscope for the surface replicas, and by means of image analysis software for the digital microscope images.

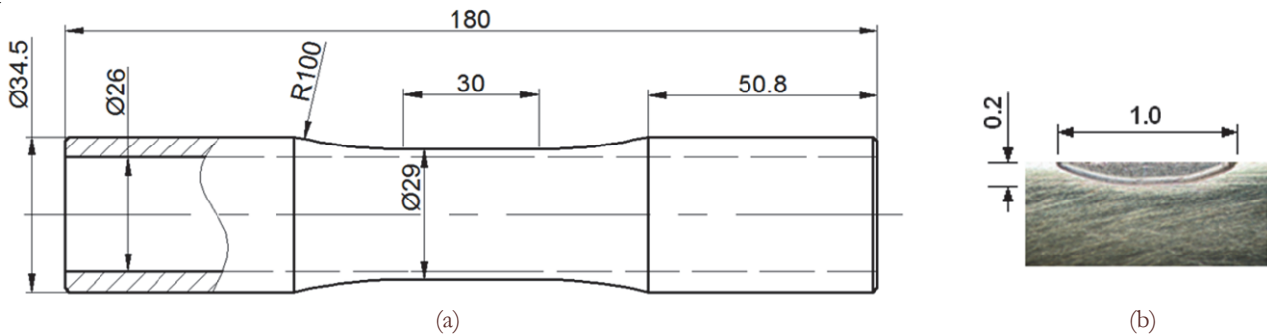


Figure 1: Test specimen details for (a) thin-walled tubular specimen geometry and (b) sectioned view of machined precrack notch. All dimensions are in mm.

All tests were performed in load control and include fully-reversed ($R = -1$) pure torsion and in-phase axial-torsion tests for both smooth and precracked specimens. Additional smooth specimen tests were also performed for pure torsion loading, with and without the addition of a static tensile or compressive stress, to evaluate the effect of mean stresses on mode II crack growth.

EXPERIMENTAL RESULTS AND DISCUSSION

Although surface replicas have shown the development of small microcrack networks in a number of the smooth specimen fatigue tests performed in this study, crack coalescence was only observed in a limited number of these tests and usually occurred relatively early in the crack growth life. Therefore, questions were raised on whether or not crack coalescence played a large role in determining overall crack path for these tests. Thus the effect of microcrack networks and coalescence was investigated through the testing of smooth and precracked specimens under identical loading conditions. Two load levels each were used for tests under fully-reversed pure torsion loading, in-phase axial-torsion loading, pure axial loading, and 90° out-of-phase axial-torsion loading. However, results from the latter two loading conditions are not included in this study because the difference between mode I and mode II growth cannot be observed from the outer surface of the specimen. A future three-dimensional analysis would be required to interpret those results. Therefore, only the experimentally observed crack paths for the two torsion loading levels and two in-phase axial-torsion load levels are shown in Fig. 2.

By comparing crack paths between the smooth and precracked specimens in Fig. 2, it is easy to see that they are very similar. This is true even for complex crack paths where cracks initiate in mode II, branch into mode I cracks, and eventually transition back to mode II after growing for some distance (Fig. 2(b-d)). This suggests that microcrack networks and their coalescence did not play a significant role in determining the crack paths for these tests. If dominant cracks, growing without the influence of crack coalescence, were expected to always branch into mode I growth regardless of the applied loading (as predicted by traditional crack growth direction criteria), then the crack path for the precracked specimen subjected to the higher level pure torsion load (Fig. 2(a)) would certainly not have remained vertical for its entire growth life. This, combined with the transition back to shear-mode growth after a period of mode I growth observed for the other precracked specimen tests, supports findings from many smooth specimen surface replicas where shear dominated crack growth occurred even in the absence of any observable crack coalescence.

Although the existence of the type R crack growth mechanism is certainly not being rejected, it is clear that in the case of this study, coalescence was most likely not responsible for the shear dominated crack paths observed in the smooth specimen tests. Therefore, there must be some other mechanism by which crack growth behavior transitions from being mode I to mode II dominated. By studying the crack paths in Fig. 2, a correlation between the loading level and/or SIF and the crack growth direction is observed. To help illustrate this point, Tab. 1 was constructed and contains all available

crack orientation data from pure torsion, torsion with static axial stress, and in-phase axial-torsion fatigue tests of smooth specimens. Nominally applied loadings are given along with shear stress amplitude and maximum normal stress on the maximum shear plane. Specimen suffixes indicate the loading conditions as follows: ST are pure torsion tests, STSA are torsion tests with static axial stress, and SC are in-phase axial-torsion tests. The table is sorted based on decreasing shear stress amplitude on the maximum shear plane. Within each shear stress level, tests are sorted by decreasing level of maximum normal stress on the maximum shear plane. Approximate crack plane orientation is then listed for different ranges of overall tip-to-tip crack length, $2c$ (in mm), as well as the total number of cycles to failure, N_f , at which point the final crack lengths were approximately 15-20 mm.

The dependence of crack growth direction on loading level is easy to see from Tab. 1. Above a shear stress amplitude of 188 MPa, all significant ranges of crack growth for all loading conditions took place in mode II on planes of maximum shear. Below this level, cracks begin to transition to mode I growth shortly after initiation and continue growing in mode I until near failure. The only exception to this trend comes when a tensile normal stress exists on the maximum shear plane. In these cases, cracks spend more time in mode II growth than specimens tested at the same shear stress amplitude without a tensile normal stress. In all but one case, both crack initiation and final failure were observed to be shear-mode processes.

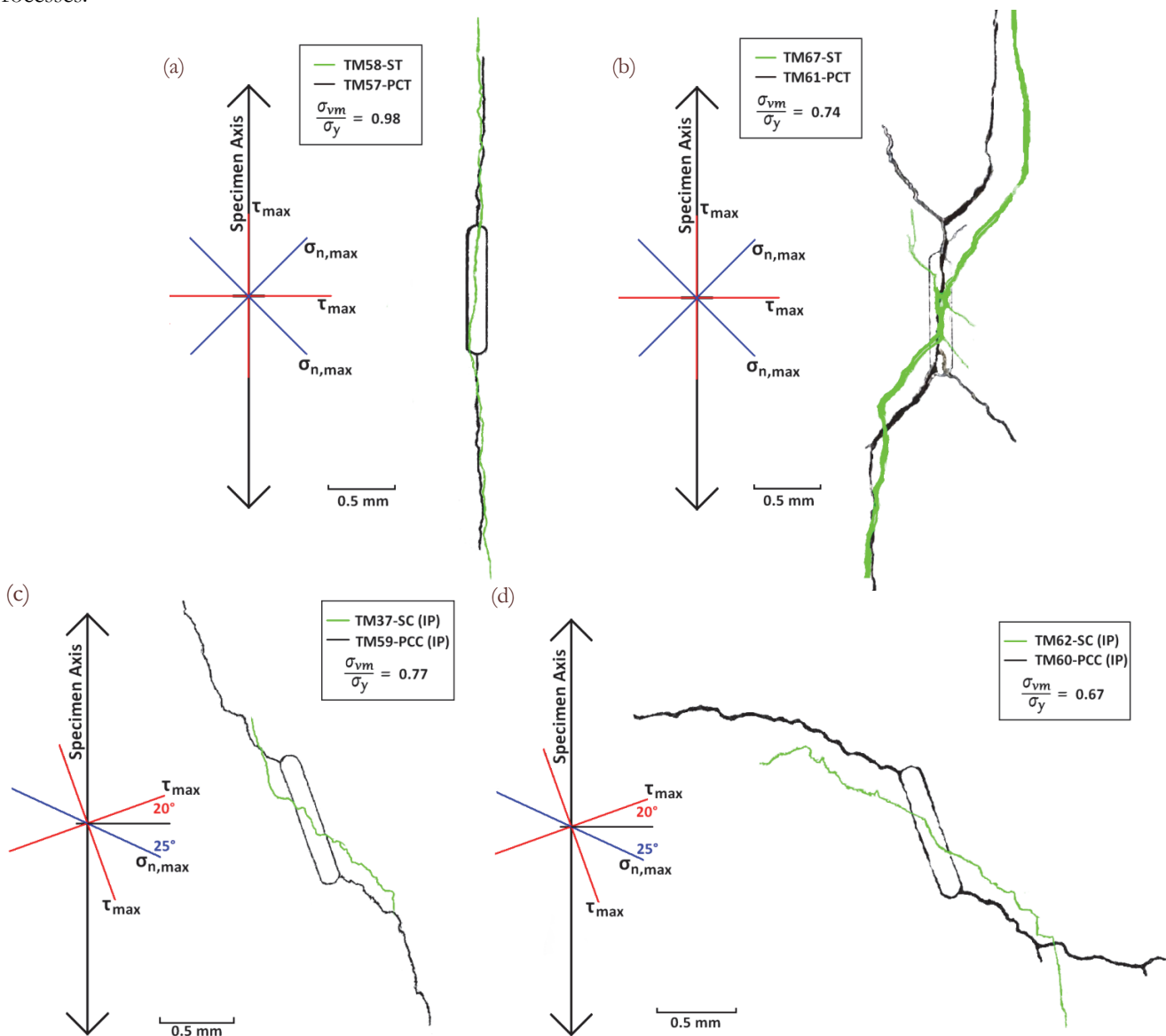


Figure 2: Superimposed crack paths for precracked specimens (black) and smooth specimens (green) tested under identical loading conditions for (a) higher load level pure torsion, (b) lower load level pure torsion, (c) higher load level in-phase axial torsion, and (d) lower load level in-phase axial-torsion tests. Relative load level is indicated by the ratio of von Mises equivalent stress to yield strength.



Specimen ID [†]	Nominal Loading (MPa)			On τ_{\max} plane (MPa)		Crack Orientation vs. Length (mm)				N_f
	τ_{amp}	σ_{amp}	σ_{mean}	τ_{amp}	σ_{max}	initiation	0.2 <2c <1	1 <2c <2	2c >2	
TM56-ST	248.3	0	0	248.3	0	τ_{\max}	τ_{\max}	τ_{\max}	τ_{\max}	736
TM63-SC	178.0	300.0	0	232.8	150.0	τ_{\max}	τ_{\max}	τ_{\max}	τ_{\max}	2009
TM100-STSA	187.8	0	92.0	187.8	92.0	τ_{\max}	τ_{\max}	τ_{\max}	τ_{\max}	6742
TM101-STSA	187.8	0	92.0	187.8	92.0	τ_{\max}	τ_{\max}	τ_{\max}	τ_{\max}	15177
TM1-ST*	187.8	0	0	187.8	0	τ_{\max}	τ_{\max}	τ_{\max}	τ_{\max}	72397
TM58-ST	187.8	0	0	187.8	0	τ_{\max}	τ_{\max}	τ_{\max}	τ_{\max}	68105
TM103-STSA	187.8	0	-92.0	187.8	0	τ_{\max}	τ_{\max}	τ_{\max}	τ_{\max}	15283
TM106-STSA	187.8	0	-92.0	187.8	0	τ_{\max}	τ_{\max}	τ_{\max}	τ_{\max}	21191
TM53-SC*	130.3	225.0	0	172.1	112.5	τ_{\max}	σ_1	τ_{\max}	τ_{\max}	25555
TM4-ST	168.2	0	0	168.2	0	τ_{\max}	σ_1	σ_1	τ_{\max}	180288
TM78-ST	150.1	0	0	150.1	0	τ_{\max}	σ_1	τ_{\max}	τ_{\max}	181299
TM96-STSA	140.3	0	150.0	140.3	150.0	τ_{\max}	τ_{\max}	τ_{\max}	τ_{\max}	35095
TM99-STSA	140.3	0	150.0	140.3	150.0	τ_{\max}	τ_{\max}	τ_{\max}	τ_{\max}	58046
TM67-ST	140.3	0	0	140.3	0	τ_{\max}	σ_1	σ_1	τ_{\max}	531716
TM105-STSA	140.3	0	-150.0	140.3	0	τ_{\max}	σ_1	σ_1	τ_{\max}	770431
TM37-SC	106.4	175.0	0	137.8	87.5	τ_{\max}	σ_1	τ_{\max}	τ_{\max}	147725
TM54-SC	90.3	156.0	0	119.3	78.0	σ_1	σ_1	σ_1	σ_1	213138
TM62-SC	90.3	156.0	0	119.3	78.0	τ_{\max}	σ_1	σ_1	τ_{\max}	867295

[†]Suffix indicates loading condition as follows: ST (pure torsion), STSA (torsion with static axial stress), and SC (in-phase axial-torsion)

*crack orientations refer to a secondary crack, not the failure crack

Table 1: Loading conditions, crack orientation vs. crack length, and fatigue life (to crack lengths of approximately 15-20 mm) for smooth specimen fatigue tests. All stresses are given in MPa and all crack lengths are given in mm.

These observations support the idea that friction and roughness induced crack closure, caused by crack face interaction, play a key role in determining crack path. At the lower loading levels, the combined effect of friction and roughness seem to reduce the effective mode II driving force at the crack tip until it drops below a critical level. This critical level could either represent a mode II threshold condition, or a value at which the potential for mode I growth exceeds that of the existing mode II crack. At this point, the crack then turns to maximum tensile planes where there is less resistance to mode I crack propagation. This idea echoes the conclusions drawn in several of the studies reviewed in the introduction. At the higher loading levels, however, these factors do not appear to play as large of a role in determining crack path. This is likely due to a combination of factors. For example, at higher stress levels, the effect of friction may not be large enough to drop the effective mode II driving force below its critical value. Additionally, increased plasticity at the crack tip can result in the deformation and destruction of the crack face asperities which would otherwise restrict the effective mode II driving force. Fig. 3 shows that as the shear stress amplitude was increased in the pure torsion tests, a longer mode II crack length was observed before branching occurred. This trend was also reported in Refs. [8, 18] and suggests that the mode II driving force increases at a faster rate than the attenuation effect due to crack face interaction, which eventually leads to a non-branching condition.

Such a dependence on load level is consistent with the observed differences between crack paths in smooth and notched specimens. Because of the stress concentration effect in notched specimens, they are often tested at much lower nominal stress amplitudes than smooth specimens. Therefore, once an initial mode II crack propagates out of the notch affected zone and into the lower stressed gage section, frictional effects would significantly restrict its growth and lead to a tendency for the crack to transition into mode I where there is less resistance to crack extension. The same is true for crack growth tests where crack growth is evaluated from a precrack. Because data for a large range of growth rates and stress intensity factors are typically desired in these types of test, they are performed at the lower nominal loadings conducive to mode I growth.

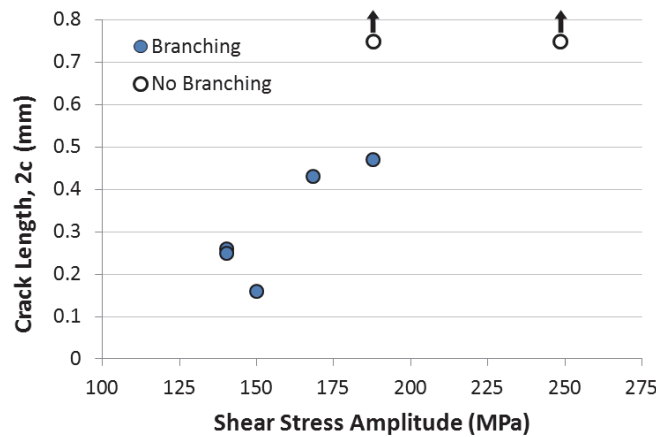


Figure 3: Initial mode II crack length before mode I branching vs. shear stress amplitude for fully-reversed pure torsion tests. Vertical arrows indicate a non-branching condition.

The mean stress effect on crack path that was observed in these tests further emphasizes the role of crack face interaction in the crack growth process. For two different values of shear stress amplitude, specimens were tested with a static compressive stress, no normal stress, and a static tensile stress. It should be noted that static normal stresses were used so as to not introduce mixed-mode growth effects through a nonzero mode I SIF range. The fatigue lives for these tests, to various tip-to-tip crack lengths, are shown in Fig. 4. For both shear stress levels, the addition of the tensile normal stress reduced the overall fatigue life by around an order of magnitude. Much of this difference can be attributed to a decrease in crack growth life which would logically stem from a reduction in crack face friction and roughness induced closure effects. As a result, crack paths for these tests were always observed to be in the specimen circumferential direction, perpendicular to the applied tensile stress (Fig. 5(a)).

For the tests in which a static compressive stress was applied, the crack growth plane switched from the specimen circumferential direction to the longitudinal direction (Fig. 5(b)). Although both are planes of maximum shear stress, the compressive normal stress acts to increase crack face interaction and inhibit crack growth on the circumferential plane. As a result, longitudinal cracks developed and grew under the same nominal loading and in a similar manner to those for torsion only tests. For specimens tested at the lower shear stress amplitude, crack branching and mode I growth was observed over the same range of crack lengths for both the compressive normal stress and pure torsion cases (although not for the specimen pictured in Fig. 5). The decrease in fatigue life observed in Fig. 4(b) for the static compression tests compared to pure torsion tests may be due to an increase in plastic zone size and crack driving force as a result of the additional compressive tangential stress (T-stress) at the crack tip. Although also present for tests performed at the lower shear stress amplitude, the effect of T-stress is expected to have a larger effect as stress levels increase. Also, the addition of the static stresses at the higher shear stress amplitude results in a general yielding condition throughout the specimen gage section which greatly increases the probability of crack initiation compared to the pure torsion test. For the lower shear stress amplitude, all loading conditions result in nominally elastic stresses throughout the gage section.

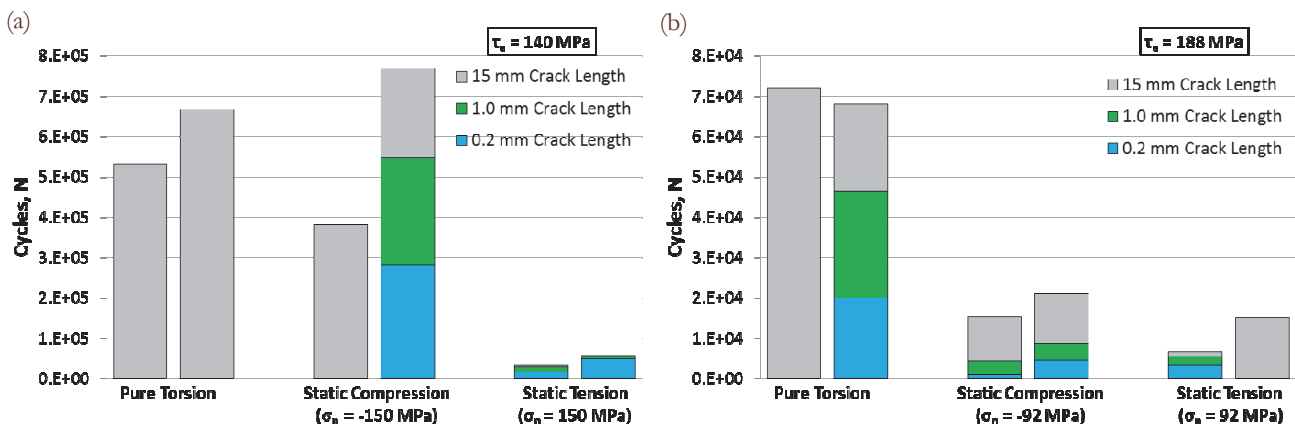


Figure 4: Fatigue lives to various crack lengths for smooth specimens tested at shear stress amplitudes of (a) 140 MPa and (b) 188 MPa with and without static axial stresses. Specimens for which no crack growth data were available are shown as solid gray columns.

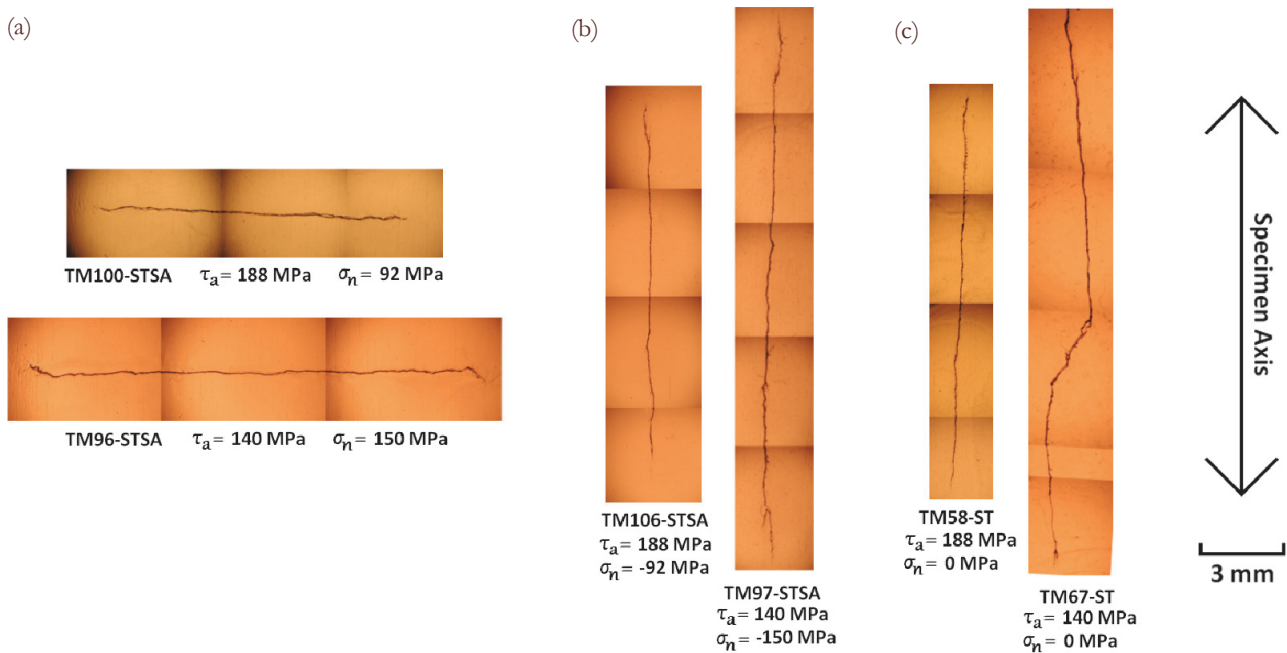


Figure 5: Final crack paths for selected smooth specimen tests under (a) torsion with static tensile stress, (b) torsion with static compressive stress, and (c) pure torsion loadings.

MODELING OF FRICTION EFFECTS

As evidenced by the experimental results, the role of friction and roughness induced closure effects on mode II crack growth is a complex, yet significant, issue. Because of the many factors involved and their inherent variability, quantification of these effects is challenging. This section will aim to reproduce some of the crack growth trends observed in experiments by presenting a simplified model to predict and quantify crack growth attenuation due to crack face friction and roughness.

The proposed model takes as its starting point the idea that friction and roughness induced crack face interaction allow a portion of the nominally applied loading to be transferred through a crack. Consider two extremes for pure torsion loading: an uncracked volume of material can transmit all of the nominal loading and creates no stress concentration effect, while a geometrically ideal mode II crack cannot transfer any load between crack faces and produces the theoretical mode II SIF value at its crack tip. Therefore, it would seem logical that an effective mode II SIF could be determined by taking into account the amount of loading transferred between crack faces in an actual cracked component. The model should be able to account for experimentally observed trends such as normal stress effect and loading level dependence and should also depend on quantities relative to crack face friction and roughness such as coefficient of friction and crack face asperity angle. For ease of implementation, it should also ideally only depend on readily available material properties and not require the use of geometry dependent functions, other than those used in SIF calculations.

In order to compute the proposed effective mode II SIF, the first step is to determine the nominal stress state. Nominal, in this case, refers to the stress state that would exist in the volume of material surrounding a crack if the crack were not present. This is assumed to be a two dimensional stress state aligned with the direction of overall crack growth. Loads transferred through the crack face are considered on an averaged basis along the entire length of the crack. If significant stress gradients exist along the length and/or depth of the crack, average stress values should be considered. The nominal coordinate system (x - y) is shown schematically in Fig. 6 along with other expressions relevant to the following discussions.

Once the appropriate stress state is known, it is transformed into a coordinate system (subsequently named x' - y') aligned with the average effective crack face asperity angle, α_{eff} , the calculation of which will be explained later. Of the stresses in the transformed coordinate system, the crack can only directly transfer a compressive stress, σ_x , normal to the asperity face. However, a resulting friction induced stress component allows for additional loads to be transferred as well. It should be noted that the model will not correctly predict frictional attenuation for asperity angles exceeding 45° . Above this angle, attenuation starts to become more of a function of mechanical interlocking than friction. Additionally, shielding from the alternating asperity angles will begin to have an effect on stresses at the crack interface above this angle.

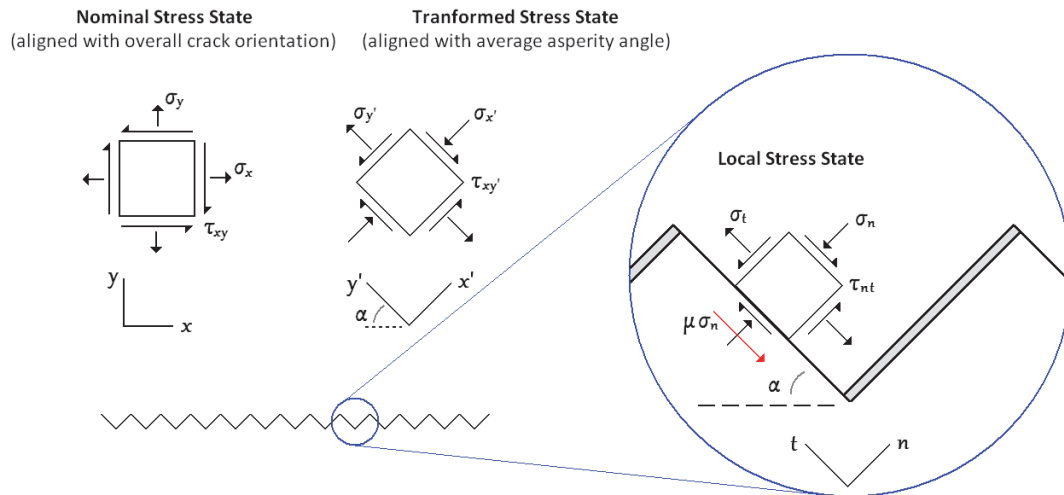


Figure 6: Schematic showing coordinate systems and nomenclature relevant to the proposed frictional attenuation model

The friction stress acting at the crack interface is calculated by multiplying the compressive normal stress, $\sigma_{x'}$, by a coefficient of friction, μ , which represents the friction between opposing crack faces under ideal contact conditions. Coefficients of friction for various materials can be readily found in machinery handbooks such as [24] and typical reported values for static coefficients include 1.1-1.3 for aluminum on aluminum contact, 0.7-0.8 for steel on steel, and 1.0 for copper on copper. Although sliding coefficients of friction are harder to find, typical values range from 50-80% of the value of the static coefficient for the same material. Since relative motion occurs between crack faces in mode II crack growth, a sliding coefficient of friction should be assumed.

This friction stress then serves to react all or part of the transformed shear stress, $\tau_{xy'}$. If the value of the friction stress is greater than the transformed shear stress, then the entire value of $\tau_{xy'}$ is considered to be acting at the crack interface as the local shear stress component, τ_{nt} . If the available friction stress is less than the transformed shear stress, on the other hand, then τ_{nt} assumes the value of the friction stress. However, if local normal stress component, $\sigma_{x'}$, is tensile, then no contact occurs between opposing crack faces, no load is transferred through the crack, and both σ_n and τ_{nt} are zero. Additionally, because crack faces perpendicular to local stress component $\sigma_{y'}$ are not in contact, this stress component is not transferred through the crack (i.e. $\sigma_t = 0$). This can be expressed mathematically by Eqs. (1) and (2):

$$\sigma_n = \begin{cases} \sigma_{x'} & \text{if } \sigma_{x'} < 0 \\ 0 & \text{if } \sigma_{x'} \geq 0 \end{cases} \quad (1)$$

$$\tau_{nt} = \begin{cases} 0 & \text{if } \sigma_{x'} \geq 0 \\ -\mu \sigma_{x'} \frac{\tau_{xy'}}{|\tau_{xy'}|} & \text{if } \sigma_{x'} < 0 \text{ and } -\mu \sigma_{x'} \leq |\tau_{xy'}| \\ \tau_{xy'} & \text{if } \sigma_{x'} < 0 \text{ and } -\mu \sigma_{x'} > |\tau_{xy'}| \end{cases} \quad (2)$$

The Macaulay brackets in Eq. (2) represent the following function: $\langle x \rangle = (x + |x|)/2$.

By taking the local crack face stress components, in $n-t$ coordinates, and transforming them back into the original $x-y$ coordinate system, a new shear stress component, τ_{frict} , can be obtained. This quantity reflects the portion of the nominally applied shear stress that is transferred through the crack due to friction and crack roughness. Therefore, an effective shear stress value, τ_{eff} , can be calculated by subtracting the frictional shear stress from the nominal value, i.e. $\tau_{eff} = \tau_{xy} - \tau_{frict}$. This effective value of shear stress is then used to compute the effective mode II SIF acting at the crack tip.

To this point, the proposed model only relies on two parameters in addition to the nominal loading: the average effective crack face asperity angle and the coefficient of friction. The coefficient of friction is assumed to be a constant, while the average effective asperity angle is allowed to evolve in order to reflect changes in crack face contact conditions. An equation describing the variation in effective asperity angle is proposed as follows:



$$\alpha_{eff} = \alpha \left(1 - e^{-\left(\frac{c}{2l}\right)^4} \right) \left\langle 1 - \beta \frac{K_{q,nom}}{K_{IC}} \right\rangle \quad (3)$$

where α is the natural/undeformed asperity angle, c is the crack length, l is a material characteristic length, $K_{q,nom}$ is the nominally applied equivalent SIF (not accounting for friction effects), K_{IC} is the material plane-strain fracture toughness, and the parameter, β , describes the influence of loading level on crack face interaction. Although Eq. (3) is phenomenological in nature, it is designed to reflect the complex changes that occur at the crack interface as a crack grows and provides a simple means of quantifying these changes.

The undeformed asperity angle, α , is independent of the applied loading and can either be determined through experimental measurements or estimated based on crystallographic structure [10]. Assuming a constant value of average asperity angle, however, would result in a nearly constant frictional effect on effective shear stress. In reality, variations in asperity angle will cause the value of friction stress to change, which will affect the load transfer through the crack interface. This phenomenon is reflected in the current model through a variation in asperity angle with crack length. The idea behind the first bracketed term in Eq. (3) is that initially, when cracks are on the order of a grain size or two, there is not much deviation in their ideal path. This is because there has not been a sufficient amount of growth to encounter slip system misalignment from one grain to the next and/or other microstructural obstacles which lead to crack meandering and the development of crack face asperities. Therefore, the effective asperity angle at zero crack length is reduced to zero by this term and allowed to gradually increase with crack length until it approaches its saturated value at a length equal to that of a few grains. This produces a behavior which agrees with the decreasing crack growth rates observed for short cracks in the constant SIF controlled tests reported in Ref. [11]. The material characteristic length, l , can be considered equal to the average grain size in the direction of crack growth.

Similarly, long cracks may also experience a reduction in frictional stresses due to changes in crack face asperities. Unlike short cracks, however, these changes are brought about as a result of asperity destruction due to plasticity and fretting along the crack interface. Additionally, the coefficient of friction is more prone to a reduction in long cracks as well, due to the formation of oxide and/or debris layers between crack faces. Since the effects of these processes generally increase with an increase in local stresses and/or crack length, the second bracketed term in Eq. (3) reflects changes in frictional attenuation by decreasing the effective asperity angle as the ratio of nominal SIF to fracture toughness increases. A linear relationship was chosen based on trends reported in Ref. [25].

The application of this model is fairly straight forward in cases of fully-reversed pure torsion loading, but it can also be applied to cases where nonzero mean and/or mixed-mode loading conditions exist. Because it is based on the stress state at the crack location, it is applicable to any type of loading and the predicted frictional attenuation is sensitive to both the applied shear stress and normal stress components. A simple Mohr's circle analysis reveals that the model will correctly predict a decrease or increase in crack face interaction due to the presence of an applied tensile or compressive stress, respectively. For situations where loading is not fully reversed, the model can be applied at both the minimum and maximum loadings in a cycle to compute the effective SIF range. However, care should be taken when determining the sign of the stress transformation angle to ensure that the transformed stress, σ_x , is perpendicular to the appropriate crack interface (related to the shear stress direction on crack growth plane) at each loading state considered.

COMPARISONS WITH EXPERIMENTAL RESULTS

Regardless of how well a model qualitatively agrees with experimental observations, its real value comes from the ability to predict crack growth behavior in a quantitative manner. The following section will evaluate the proposed model's ability to do so by analyzing the experimental data presented earlier. Correlations will be made concerning both crack branching and crack growth rate. Due to time constraints, however, the analysis presented in this section is only applied to situations involving fully-reversed pure torsion loadings. The effectiveness of the model when applied to situations involving static axial stresses or mixed-mode loadings will be evaluated in a future study.

The first step in analyzing the experimental data was to gather the relevant material parameters for the proposed model. The average undeformed crack face asperity angle was measured from the surface crack replicas of several specimens when crack lengths, $2c$, were less than 1 mm. Fifteen measured values ranged from 16° to 60° with an average of 36° and standard deviation of 14° . A value for sliding coefficient of friction under ideal conditions could not be found and was instead estimated as being 0.67 times the average reported static values for aluminum on aluminum contact, i.e. $0.67(1.2)$



$= 0.8$. The parameter, β , in Eq. (3), was assumed to be 4 loosely based on data and trends reported in Ref. [24]. This predicts that the frictional attenuation due to crack face interference disappears after the nominal SIF exceeds one quarter of the value of the material's plane-strain fracture toughness. The value for latter was considered to be $34 \text{ MPa}\sqrt{\text{m}}$ [26] and an average grain size of 0.075 mm was used based on data reported in Ref. [27] for 2024-T3 aluminum alloy. To compute nominal and effective SIF values, the ideal mode II crack geometry was considered to be a semi-elliptic surface crack in a finite thickness plate growing with a constant aspect ratio (a/c) of 0.5. This aspect ratio corresponds to a condition where the mode II SIF at the specimen surface is approximately equal to the mode III SIF at the crack's maximum depth, a , [28]. Therefore, an ideal crack growing in shear-mode would be expected to maintain this aspect ratio throughout its growth life. This agrees well with the experimental crack shape data presented in Ref. [29] for pure torsion loading of Inconel 718. With this aspect ratio, cracks do not become through thickness for any of the LEFM applicable crack lengths considered in this analysis. Appropriate geometry factor functions were obtained through the fitting of linear FEA results, derived using the XFEM crack technique in Abaqus/CAE 6.11-1, for several crack lengths. With all of the model inputs known, calculations for effective mode II SIF were carried out using the previously described procedure. Since the loading considered was fully reversed, SIF values were only calculated at the maximum applied loading and were doubled to obtain the effective mode II SIF range. Fig. 7 shows crack growth rate versus both the nominally applied and effective mode II SIFs calculated for all available LEFM applicable pure torsion crack growth data. Growth rates were computed using a three point polynomial reduction technique. It can be seen from the figure that the model predicts a significant effect from frictional attenuation on the effective SIF values while at the same time improving correlation between the various loading levels. The effective SIF decreases by around a factor of 3 at the lower crack growth rates and begin to merge with the nominal values at around 10^{-7} m/cycle . Reductions in effective SIF of a similar order were measured experimentally in Refs. [20, 30].

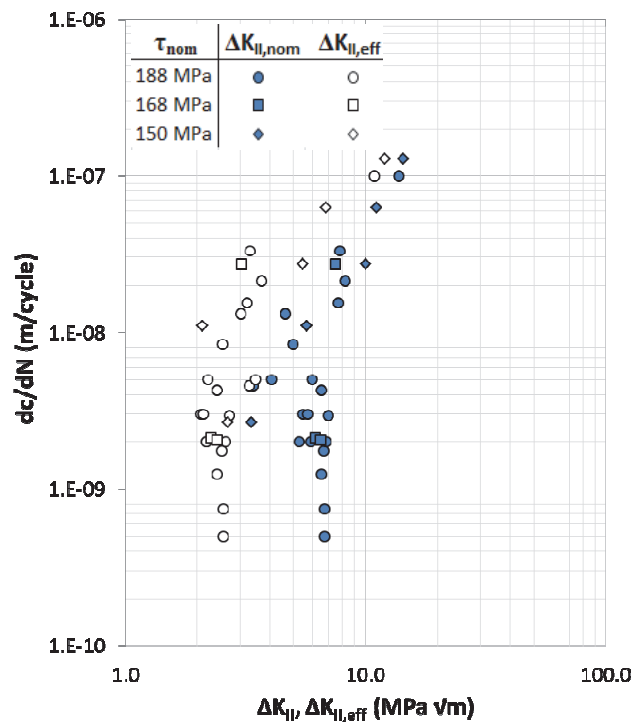


Figure 7: Experimentally measured LEFM applicable crack growth rates vs. nominal and effective mode II SIF for fully-reversed torsion tests.

Another application of the proposed model is in predicting whether or not crack branching will occur for a given loading condition. In order to do this, the effective mode II SIF value must be compared to a crack branching criterion. For this analysis, a maximum growth rate criterion was considered and was evaluated at the outer surface location of the specimen where the growth is pure mode II. Since reliable data on crack growth kinetics (in the absence of closure effects) were not readily available for the tested material, an equivalent SIF formulation was used as the basis to compare crack growth potential for each mode. Equivalent SIF was computed using Eq. (4), which is based on the summation of energy release rates due to each crack extension mode:



$$\Delta K_q = \sqrt{\Delta K_I^2 + \Delta K_{II}^2 + (1+\nu)\Delta K_{III}^2} \quad (4)$$

According to this equation, mode I and mode II SIFs have the same contribution to the equivalent SIF value. Therefore, for this analysis, whichever loading mode produced the highest SIF was considered the preferred crack growth mode.

Mode I SIF values were based on the normal stress component, as calculated from the nominally applied stresses, acting on the maximum principal stress plane at the location of the crack. To account for differences in effective crack length due to plane orientation, the overall crack length was projected onto the maximum principal plane prior to calculating the mode I SIF. Only the tensile portion of the normal stress cycle was considered for the calculation of SIF range, as the crack is assumed to be closed under compression. The mode I geometry factor function was obtained using the same crack geometry and procedures described for mode II. Although there is likely some degree of error in these calculations due to the difference in profile between the projected crack and an ideal mode I crack, this effect has not yet been evaluated.

Fig. 8 shows analysis results for the four different LEFM applicable pure torsion loading levels applied in the experimental program. Each plot shows the effective mode II SIF range, computed using the proposed model, along with the mode I potential SIF range versus half crack length. The effective asperity angle is also plotted for reference. The vertical dotted lines on each plot enclose the regions of experimentally observed mode I growth for each loading level and experimental mode II growth regions are highlighted in red. By studying this figure, it can be seen that this type of analysis is able to reflect the trend observed in Fig. 3 of an increase in initial mode II crack length before branching with increasing loading level. Additionally, the predicted crack length at this transition is within a factor of 2.5 of the experimentally measured value for all loadings cases considered. It is also worth noting that a further increase in applied loading would have resulted in the correct prediction of a non-branching crack condition and that a transition back to shear-mode growth after a period of mode I growth, which was observed in experiments, was predicted by the analysis. Although in the latter case, quantitative results can vary due to the potential for a mode I branch to cause significant deviation from the idealized mode II path assumed by the model. Fig. 9 shows a fairly reasonable agreement between the experimental and predicted crack paths for the fatigue tests represented in Fig. 8(a) and 8(c).

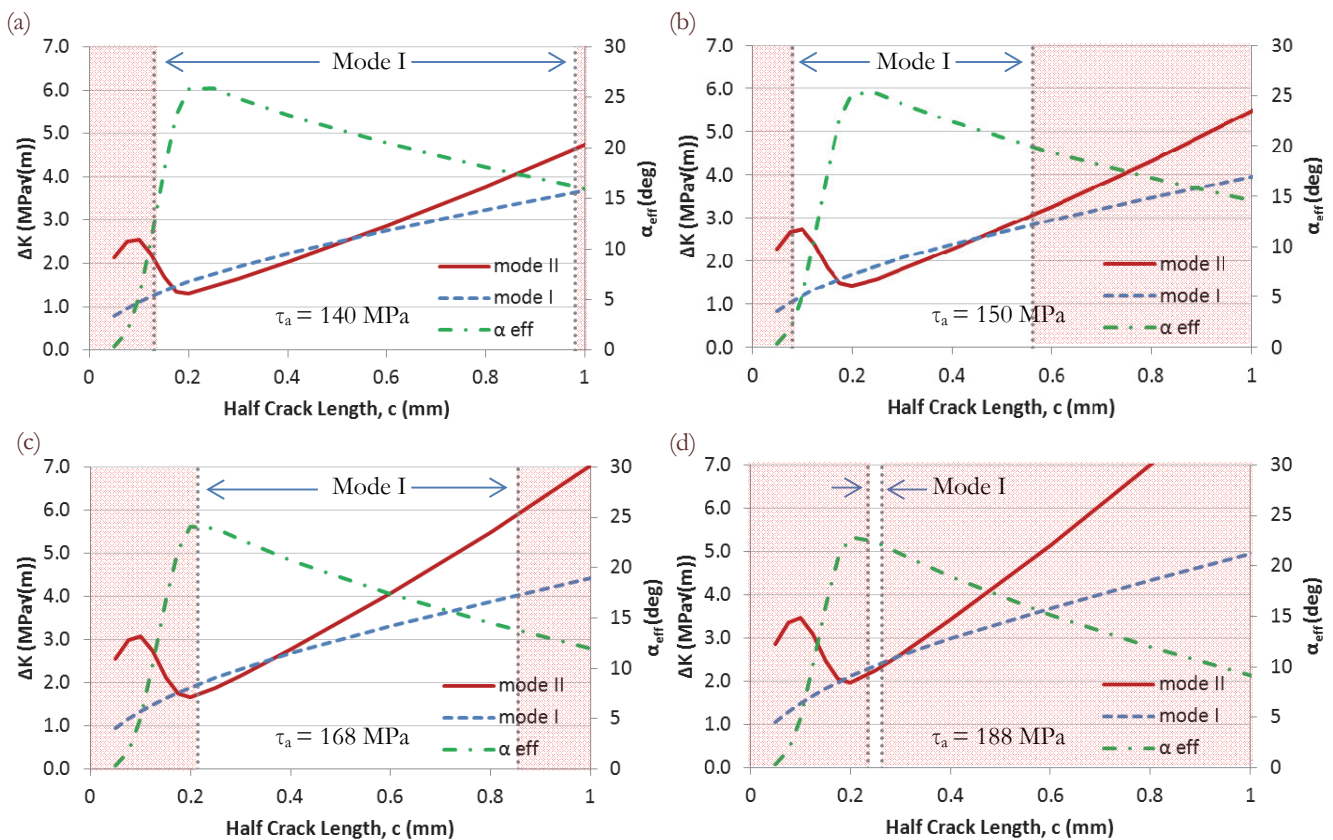


Figure 8: Effective mode II SIF, local mode I SIF, and effective coefficient of friction vs. crack length for fully-reversed pure torsion loadings of (a) 140 MPa, (b) 150 MPa, (c) 168 MPa, and (d) 188 MPa. All results represent LEFM applicable regions of crack growth.

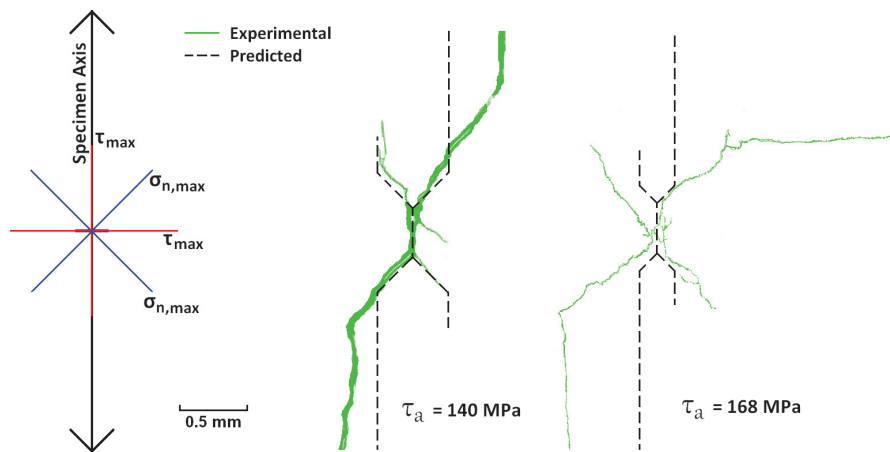


Figure 9: Experimental vs. predicted crack path based on maximum growth rate criterion and proposed crack friction model.

These initial results are promising because they demonstrate the ability of the proposed model to predict experimentally observed trends in shear-mode crack growth. However, because this model is new, further investigation is needed to determine its robustness and general applicability. Future application to the torsion with static axial and in-phase axial-torsion data presented in this study will provide a means for some of this verification, but additional analyses for different materials and loading conditions would be necessary as well. In addition, a preliminary analysis of the sensitivity of the model to the various input parameters indicates a fairly strong dependence on the β value, a more moderate dependence on coefficient of friction and asperity angle, and a smaller effect of the average grain size only at shorter crack lengths. A more in depth sensitivity study should be performed as well to help quantify these effects.

CONCLUSIONS

Despite the significance of shear-mode crack growth mechanisms and crack branching phenomena in practical applications, relatively little research is available regarding these topics. Of the studies that have been performed, few provide a means of quantifying such effects and even fewer consider the natural initiation of fatigue cracks in smooth specimens. The current study was aimed at trying to fill some of the research voids in these areas. Based on the experimental results and analysis presented herein, the following conclusions can be drawn:

1. Microcrack networks and coalescence do not appear to have an effect on the experimentally observed crack paths for the smooth specimen fatigue tests performed in this study, regardless of the applied loading level.
2. The preferred crack growth mode is shown to have a dependence on the applied shear stress magnitude as well as the stress normal to the crack plane. This indicates that friction and roughness induced crack closure effects play a significant role in the shear-mode crack growth process.
3. An increase in initial mode II crack length before branching is observed with an increase in pure torsion loading level. This indicates that the mode II driving force increases at a higher rate than the attenuation effect due to crack face interaction, which eventually leads to a non-branching condition.
4. A simple model is proposed in an attempt to quantify the complex phenomena involved in crack growth attenuation due to friction and roughness induced closure effects. The model is based on the idea that crack face interaction reduces the effective mode II SIF by allowing a portion of the nominally applied loading to be transferred through a crack interface. Resulting crack path predictions are shown to agree relatively well, both qualitatively and quantitatively, with experimentally observed trends for pure torsion loading. Although the model shows promise for application to more complex loading conditions, more analysis is needed for such cases to verify its robustness.

REFERENCES

- [1] Carpinteri, A., Pook, L. P., Susmel, L., Vantadori, S., Fatigue crack paths 2012, *Int. J. Fatigue*, 58 (2014) 1.
- [2] Fatemi, A., Gates, N. R., Socie, D. F., Phan, N., Fatigue crack growth behaviour of tubular aluminum specimens with a circular hole under axial and torsion loadings, *Eng. Fract. Mech.*, 123 (2014) 137–147.



- [3] Tanaka, K., Small fatigue crack propagation in notched components under combined torsional and axial loading, *Procedia Eng.*, 2 (2010) 27–46.
- [4] Zhang, H., Fatemi, A., Short Fatigue crack growth behaviour under mixed-mode loading, *Int. J. Fract.*, 165 (2010) 1–19.
- [5] Qian, J., Fatemi, A., Fatigue crack growth under mixed-mode I and II loading, *Fatigue Fract. Eng. Mater. Struct.*, 19:1 (1996) 1277–1284.
- [6] Socie, D. F., Marquis, G. B., *Multiaxial Fatigue*, Society of Automotive Engineers, Inc., Warrendale, PA, (2000).
- [7] Murakami, Y., Takahashi, K., Kusumoto, R., Threshold and growth mechanism of fatigue cracks under mode II and III loadings, *Fatigue Fract. Eng. Mater. Struct.*, 26 (2003) 523–531.
- [8] Doquet, V., Bertolino, G., Local approach to fatigue cracks bifurcation, *Int. J. Fatigue*, 30 (2008) 942–950.
- [9] Tanaka, K., Small crack propagation in multiaxial notch fatigue, *Proceedings of the 4th International Conference on Crack Paths (CP 2012)*, Gaeta, Italy, (2012) 31–45.
- [10] Pokluda, J., Pippan, R., Vojtek, T., Hohenwarter, A., Near-threshold behaviour of shear-mode fatigue cracks in metallic materials, *Fatigue Fract. Eng. Mater. Struct.*, 37 (2014) 232–254.
- [11] Tschegg, E. K., Mode III and Mode I fatigue crack propagation behaviour under torsion loading, *J. Mater. Sci.*, 18 (1983) 1604–1614.
- [12] Shamsaei, N., Fatemi, A., Small fatigue crack growth under multiaxial stresses, *Int. J. Fatigue*, 58 (2014) 126–135.
- [13] Marco, S. M., Starkey, W. L., A Concept of Fatigue Damage, *Trans. ASME*, 76 (1954) 627–632.
- [14] Qian, J., Fatemi, A., Mixed mode fatigue crack growth: a literature survey, *Eng. Fract. Mech.*, 55 (1996) 969–990.
- [15] Erdogan, F., Sih, G. C., On the crack extension in plates under plane loading and transverse shear, *ASME J. Basic Eng.*, 85 (1963) 519–525.
- [16] Tanaka, K., Fatigue crack propagation from a crack inclined to the cyclic tensile axis, *Eng. Fract. Mech.*, 6 (1974) 493–507.
- [17] Murakami, Y., Takahashi, K., Torsional fatigue of a medium carbon steel containing an initial small surface crack introduced by tension-compression fatigue: crack branching, non-propagation and fatigue limit, *Fatigue Fract. Eng. Mater. Struct.*, 21 (1998) 1473–1484.
- [18] Makabe, C., Socie, D. F., Crack growth mechanism in precracked torsional fatigue specimens, *Fatigue Fract. Eng. Mater. Struct.*, 24 (2001) 607–615.
- [19] Tong, J., Yates, R., Brown, M. W., A model for sliding mode crack closure Part I: Theory for pure mode II loading, *Eng. Fract. Mech.*, 52:4 (1995) 599–611.
- [20] Tong, J., Yates, R., Brown, M. W., A model for sliding mode crack closure Part II: Mixed mode I and II loading and application, *Eng. Fract. Mech.*, 52:4 (1995) 613–623.
- [21] Künkler, B., Düber, O., Köster, P., Krupp, U., Fritzen, C.-P., Christ, H.-J., Modelling of short crack propagation - Transition from stage I to stage II, *Eng. Fract. Mech.*, 75 (2008) 715–725.
- [22] ASTM Standard E 2207-08: Standard Practice for Strain-Controlled Axial-Torsional Fatigue Testing with Thin-Walled Tubular Specimens, in: Bailey, S. J., Baldini, N. C. (Eds.), *Annual Book of ASTM Standards*, vol. 03.01, ASTM International, West Conshohocken, (2009) 1258–1265.
- [23] ASTM Standard E 1012-05: Standard Practice for Verification of Test Frame and Specimen Alignment Under Tensile and Compressive Axial Force Application, in: Bailey, S. J., Baldini, N. C. (Eds.), *Annual Book of ASTM Standards*, vol. 03.01, ASTM International, West Conshohocken, PA, (2009) 797–807.
- [24] Oberg, E., Jones, F. D., Horton, H. L., Ryffel, H. H., *Machinery's Handbook*, twenty-sixth ed., Industrial Press Inc., New York, (2000).
- [25] Doquet, V., Bertolino, G., A material and environment-dependent criterion for the prediction of fatigue crack paths in metallic structures, *Eng. Fract. Mech.*, 75 (2008) 3399–3412.
- [26] *Military Handbook: Metallic Materials and Elements for Aerospace Vehicle Structures: MIL-HDBK-5H*, United States Department of Defense, (1998).
- [27] Merati, A., A study of nucleation and fatigue behavior of an aerospace aluminum alloy 2024-T3, *Int. J. Fatigue*, 27 (2005) 33–44.
- [28] Murakami, Y., Fukushima, Y., Toyama, K., Matsuoka, S., Fatigue crack path and threshold in Mode II and Mode III loadings, *Eng. Fract. Mech.*, 75 (2008) 306–318.
- [29] Beer, T., *Crack Shapes During Biaxial Fatigue*, Report No. 106, University of Illinois at Urbana-Champaign, Urbana, IL, (1984).
- [30] Vaziri, A., Nayeb-Hashemi, H., The effect of crack surface interaction on the stress intensity factor in Mode III crack growth in round shafts, *Eng. Fract. Mech.*, 72 (2005) 617–629.